

# THz PROPERTIES OF GRATING-GATE PLASMONIC CRYSTALS

P. Sai <sup>a</sup>, M. Dub <sup>a</sup>, V. Korotyeyev <sup>a,b</sup>, S. Kukhtaruk <sup>a,b</sup>, G. Cywinski <sup>a</sup>, and W. Knap <sup>a</sup>

<sup>a</sup> *CENTERA Laboratories, Institute of High Pressure Physics PAS, 01-142 Warsaw, Poland*

<sup>b</sup> *V.Ye. Lashkaryov Institute of Semiconductor Physics (ISP), NASU, 03028 Kyiv, Ukraine*

Email: [psai@unipress.waw.pl](mailto:psai@unipress.waw.pl)

Received 10 November 2023; accepted 13 November 2023

This study reviews recent advances in the modern field of terahertz plasmonics concerning the control of resonant properties of grating-gate plasmonic crystal structures. Particularly, we conducted both experimental and theoretical investigations of AlGaIn/GaN grating-gate structures with a focus on investigations of the resonant structure of transmission spectra associated with plasmon excitations in two-dimensional electron gas at different modulation degree of concentration profiles. Two distinct resonant phases of the plasmonic crystal structure were analyzed. The first one, the delocalized phase, is observed in the case of a small modulation degree of electron gas. In this phase, we found that plasmonic resonant absorption of incident radiation occurs across the entire grating-gate structure, with domination in the gated regions of the electron gas. In contrast, the second phase, the localized one, is realized at a strong modulation of the electron concentration profiles when the gated regions of the electron gas are completely depleted. Here, plasmon resonances are characterized by the spatial localization of absorption of incident radiation exclusively within the ungated regions of the electron gas. Moreover, in the localized phase, we observed the unexpected blue shift of plasmon resonant frequency with an increase of gate voltage. This observation was explained by the result of ‘edge gating effect’ and additional shrinking of the concentration profile of the electron gas in the ungated region. We demonstrate that the correct description of both phases requires rigorous electrodynamic simulations and cannot be achieved solely in the frameworks of simplified single-mode or single-cavity models.

**Keywords:** plasmonic crystal, plasmon resonance, terahertz spectroscopy, integral equations method

## 1. Introduction

The burgeoning field of terahertz (THz) plasmonics has been invigorated by the advent of large-amplitude plasma oscillations within field-effect transistor (FET) channels, where the oscillation frequency can be precisely controlled by the gate voltage [1, 2]. Recent decades have seen a significant attention directed towards exploiting the potential of periodic structures, such as FET arrays, grating gates and multigate configurations, as they facilitate enhanced interactions between incoming electromagnetic radiation and two-dimensional (2D) plasmons. These structures have already showcased improved performance as THz detectors [3–6], and ongoing experimental efforts suggest their growing role as potential THz radiation emitters [7, 8] or amplifiers [9].

In a broader context, these periodic structures are referred to as plasmonic crystals (PCs) [10, 11]. A grating-gate PC, as illustrated in Fig. 1(a), is a meticulously designed arrangement of multiple plasmonic cavities, often achieved by positioning metallic grating gates in close proximity to a 2D electron gas (2DEG) layer. These metallic grating gates serve multiple roles: (i) control of the plasmonic cavity size, (ii) antenna coupler to ensure an efficient THz light–plasmon interaction, and (iii) 2DEG density control providing tunability of resonant properties of PC. Initially, analogous plasmonic configurations were utilized to observe 2D plasmon resonances within silicon inversion layers [12, 13]. Subsequent research endeavours have expanded to encompass diverse materials such as InGaAs/InP [14], AlGaAs/GaAs [15], AlGaIn/GaN [16, 17] and graphene structures [18, 19].

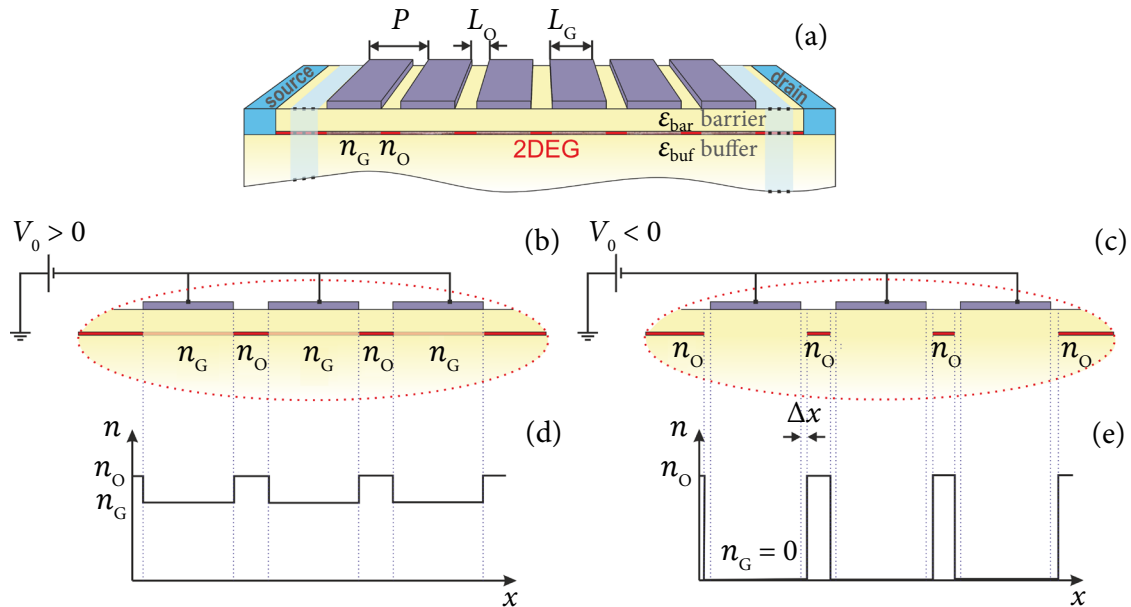


Fig. 1. Schematic view of the grating-gate PC (a) realized in the FET configuration with source, drain and grating-gate electrodes, where  $P$  is the grating period, and  $L_G$  and  $L_O$  are the lengths of gated and ungated plasmonic cavities, respectively. Panels (b) and (c) illustrate the plasmonic cavities at the applied gate voltage swing  $V_0$  in the regimes of weak and strong 2DEG density modulation, respectively. Panels (d) and (e) represent the electron concentration profiles at the gate voltage swing  $V_0 > 0$  and  $V_0 < 0$ , respectively. The  $n_G$  and  $n_O$  are 2DEG concentrations in the gated and ungated cavities, respectively.  $\Delta x$  is the additional lateral depletion of the ungated cavities in the regime of strong 2DEG density modulation.

Although many aspects of grating-gate PCs have been examined theoretically by research groups led by Mikhailov [20], Popov [21, 22] and Kochelap [23–26], a comprehensive exploration of the characteristics of these structures remains notably absent in the scientific literature. This knowledge gap can be attributed to two primary challenges. Firstly, the experimental challenge arises from the necessity of incorporating a substantial number of non-leaking gates within a single PC to effectively excite 2D plasmons within the THz range. Secondly, the theoretical challenge stems from the inherent nonuniform composition of PCs, where gated and ungated cavities coexist, and there is interaction between them. So, a theoretical description of the existing PC structures (see Fig. 1(a)) with arbitrary shapes of the grating couplers and complicated multi-layered stack geometry (in the vertical direction) cannot be reduced to any analytical expressions, and a correct description of PC resonances requires rigorous electrodynamic simulations. Consequently, the accurate prediction and interpretation of plasmonic crystal properties necessitate advanced numerical calculations.

In this work, we demonstrate the solutions for these existing challenges and investigate the AlGaIn/GaN grating-gate PCs in the regimes of weak (Fig. 1(b, d)) and strong (Fig. 1(c, e)) modulation of 2DEG density. The integral equation method (IEM) was used for the electrodynamic simulations of PC transmission spectra in the THz range. We experimentally and theoretically studied different phases of grating-gate PCs. The first phase, termed the delocalized phase, is characterized by the absorption of THz radiation throughout the entire grating-gate structure, but predominantly in the gated regions. This phenomenon manifests itself when the 2DEG density modulation is weak. In contrast, the second phase, known as the localized phase, exhibits a distinct behaviour. Here, THz radiation absorption occurs exclusively within the ungated regions of the structure. Achieving this phase requires the total depletion of the gated part of 2DEG. Notably, our investigation reveals that the transition between these phases is continuous and can be actively controlled through gate modulation of 2DEG.

Moreover, in our THz spectroscopy measurements, we observed an unexpected blue shift of

the plasmon resonant frequency of PC in the localized phase at a further increase of negative gate voltages. This intriguing phenomenon can be attributed to a specific effect, namely, the shrinking of the conductive profile of 2DEG in the ungated region. This effect of additional depletion can be called the ‘edge gating effect’ and will be described by quantity  $\Delta x$  (as depicted in Fig. 1(c, e)).

The main part of the experimental results has been published in the authors’ original prior publication [27] which will be re-reviewed and extended in their interpretations in this article. In particular, the results of the integral equation method were validated independently by the finite element method (FEM). FEM was also used for the calculations of spatial distributions of the electric field component of electromagnetic (em) wave in the near-field zone. Our observations suggest that the phenomena cannot be adequately elucidated solely through the lens of single-mode and single-cavity approximations. Instead, it becomes imperative to consider the grating-gate PC model as it offers a more comprehensive framework for explaining the observed results.

It is noteworthy that while our study is focused on a specific case involving plasmons in AlGaIn/GaN grating-gate PCs, the insights that we have gained possess a broader applicability. The general character of our results extends their relevance to other semiconductor-based plasmonic crystal structures, offering valuable implications for a broader field of THz plasmonics.

## 2. Unbiased AlGaIn/GaN grating-gate PC structures

As mentioned above, the key component of a PC structure is the metallic grating deposited on the top layer of a bare heterostructure. Different PCs with different geometries of the metallic grat-

ing were fabricated and tested. The metallic gratings were fabricated by electron-beam patterning, following Ni/Au metallization evaporation and its lift-off. The specific geometric parameters of such gratings are provided in Table 1.

The AlGaIn/GaN heterostructures used in our experiments were grown using the metalorganic vapour phase epitaxy (MOVPE) method, employing a 4-inch diameter semi-insulating SiC substrate, with a thickness of 500  $\mu\text{m}$ . That semiconductor stack was composed of a 2.4 nm GaN cap layer, a 20.5 nm  $\text{Al}_{0.25}\text{Ga}_{0.75}\text{N}$  barrier layer and a 255 nm GaN buffer layer, which was directly grown on a 62 nm-thick AlN nucleation layer situated on the SiC substrate.

In the processing of the PC structure (schematically shown in Fig. 1(a)), we especially paid attention to the technology of fabrication of large-area grating gates with minimized gate leakage currents. That was deemed critical for achieving an effective control over the 2DEG density within the PCs, especially considering their substantial active area ( $>1.7 \times 1.7 \text{ mm}^2$ ). To realize this objective, we dedicated special attention to ensuring the quality of both the Schottky barrier contact (grating-gate coupler) and the ohmic contacts for the source and drain, each of which interfaces with the 2DEG channel. For a more comprehensive description of the fabrication process for the grating-gate PCs, readers are encouraged to refer to our paper [27].

Transmission spectra measurements of the AlGaIn/GaN-based PCs were performed by a Fourier transform vacuum spectrometer (Vertex 80v from Bruker, Billerica, Massachusetts, USA) integrated with a continuous flow liquid helium cryostat. All measurements were done at 10 K. The obtained transmission spectra of all investigated samples are illustrated in Fig. 2 under the unbiased conditions of the grating electrode (zero gate voltage  $V_G = 0 \text{ V}$ ). As seen, all spectra demonstrate

Table 1. Grating-gate coupler parameters of the four investigated PC samples.

Sample ID	Grating period $P, \mu\text{m}$	Gated region width $L_G, \mu\text{m}$	Ungated region width $L_O, \mu\text{m}$	Grating filling factor $r = L_G/P$	Number of grating cells $N_{GC}$	Active area, $\text{mm}^2$
S1	1.0	0.50	0.50	0.50	1650	$1.7 \times 1.7$
S2	1.5	0.90	0.60	0.60	1100	$1.7 \times 1.7$
S3	2.5	2.15	0.35	0.86	712	$1.8 \times 1.8$
S4	3.5	3.15	0.35	0.90	508	$1.8 \times 1.8$

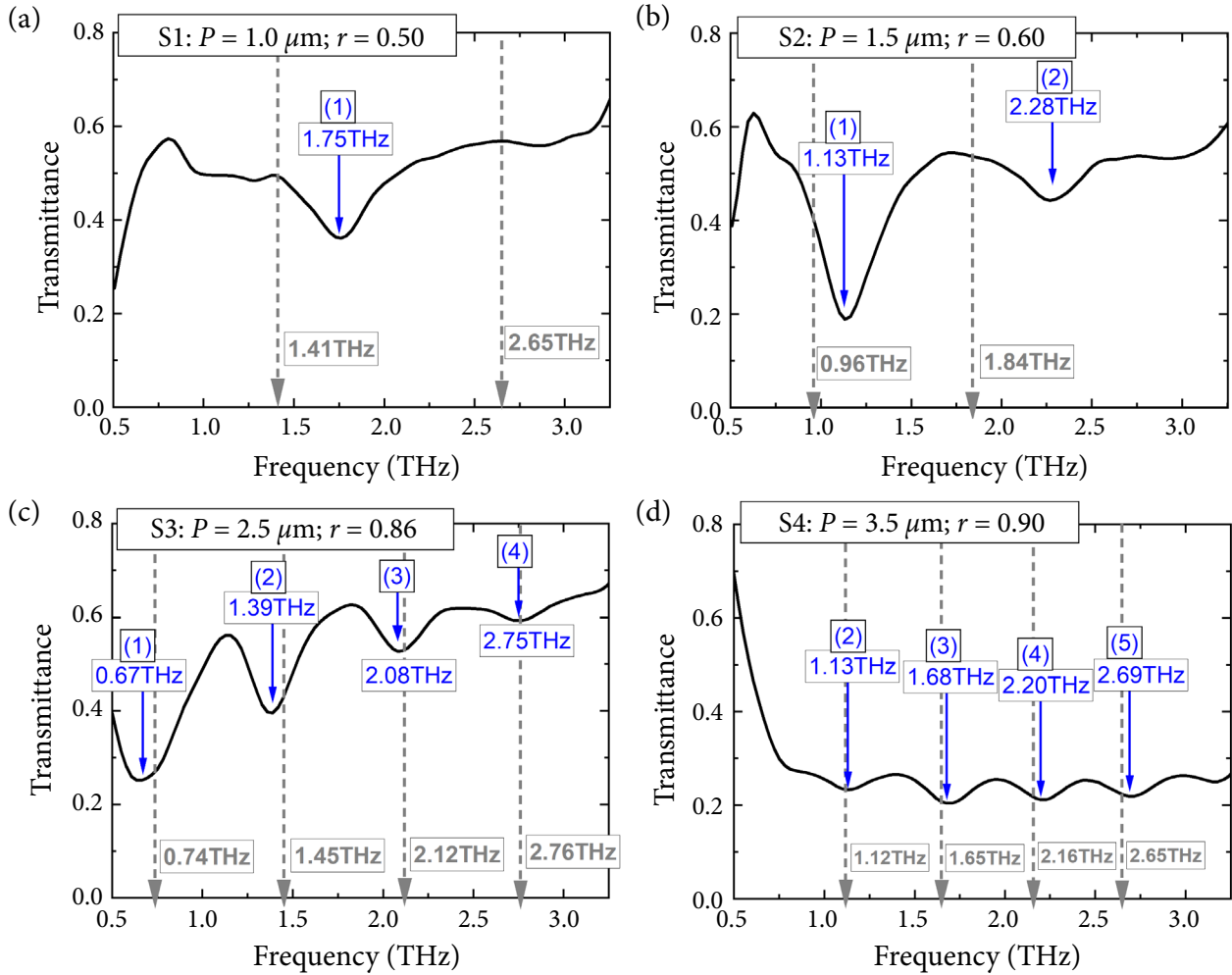


Fig. 2. THz transmittance of the unbiased PCs with a different grating period  $P$  and a grating filling factor  $r$ : (a) S1 sample:  $P = 1.0 \mu\text{m}$ ,  $r = 0.50$ ; (b) S2 sample:  $P = 1.5 \mu\text{m}$ ,  $r = 0.60$ ; (c) S3 sample:  $P = 2.5 \mu\text{m}$ ,  $r = 0.86$ ; (d) S4 sample:  $P = 3.5 \mu\text{m}$ ,  $r = 0.90$ . Blue arrows with numbers indicate the position and order of plasmon resonances extracted from the experimental spectra. Grey dashed arrows indicate the position and order of the plasmon resonances calculated by Eq. (1). All parameters of the investigated sample are listed in Table 1.

features inherent to the resonant excitations of 2D plasmon oscillation in the weakly nonuniform 2DEG.

For the qualitative estimations of the position of resonances, we can use the so-called single-mode approach based on the 2D plasmon dispersion law obtained for totally gated and ungated 2D plasmons [22, 28, 29]. When the grating-gate coupler is placed in close proximity to the 2DEG layer ( $|k|d \ll 1$ ), these dispersion relationships can be written as follows:

$$\omega_G = |k| \sqrt{\frac{e^2 n_G d}{m^* \epsilon_0 \epsilon_{\text{bar}}}}, \quad (1)$$

$$\omega_O = \sqrt{|k| \frac{e^2 n_0}{m^* \epsilon_0 (\epsilon_{\text{buf}} + 1)}}. \quad (2)$$

Here  $k$  is the plasmon wave vector,  $n_G$  and  $n_0$  are the electron concentrations (in general, they can be essentially different) in the gated and ungated regions of 2DEG, respectively,  $m^*$  is the effective electron mass,  $d$  is the thickness of barrier layer,  $\epsilon_{\text{bar}}$  and  $\epsilon_{\text{buf}}$  are the dielectric permittivities of barrier and buffer layers, respectively, and  $\epsilon_0$  is vacuum permittivity (formulas (1) and (2) are provided in SI units).

In Fig. 2, blue arrows with numbers indicate the position and order of plasmon resonances extracted from the experimental spectra. Grey dashed arrows correspond to the positions of the plasmon resonances calculated using Eq. (1). As seen, in the case of large grating filling factors  $r \rightarrow 1$  (samples S3 and S4, see Fig. 2(c, d)), the plasmon resonance frequency can be well approximated by Eq. (1) as

for totally gated 2D plasmons, taking  $|k| = 2\pi j/P$ , where ( $j = 1, 2, 3, \dots$ ) numerates the order of resonances. Here, we imply that a wave vector of the ‘resonant’ plasmons is defined by the grating periodicity. In estimations, we used the value of concentration  $n_G = 6.2 \times 10^{12} \text{ cm}^{-2}$ , extracted from DC measurements (see Section 3), the dielectric permittivity  $\epsilon_{\text{bar}} = 8.9$  and the thickness  $d = 22 \text{ nm}$ , corresponding to the AlGaIn barrier layer.

However, in the case of smaller grating filling factors (samples S1 and S2, see Fig. 2(a, b)), such a single-mode approach is not valid and this kind of grating-gate structure should be considered only in the frameworks of the plasmonic crystal model where the interaction between gated and ungated parts of 2DEG is considerable.

Below, we will focus on the analysis of a more interesting case of the S2 sample for which the single-mode approach cannot describe the positions of the fundamental and second-order plasmon resonances.

### 3. Biased AlGaIn/GaN grating-gate PC structures (S2 sample)

Grating-gate PCs were designed to provide the possibility of DC biasing to the entire grating electrode. The example of the transfer current–voltage characteristic of PC under test is illustrated in Fig. 3 (left panel) in a semilogarithmic scale. It dem-

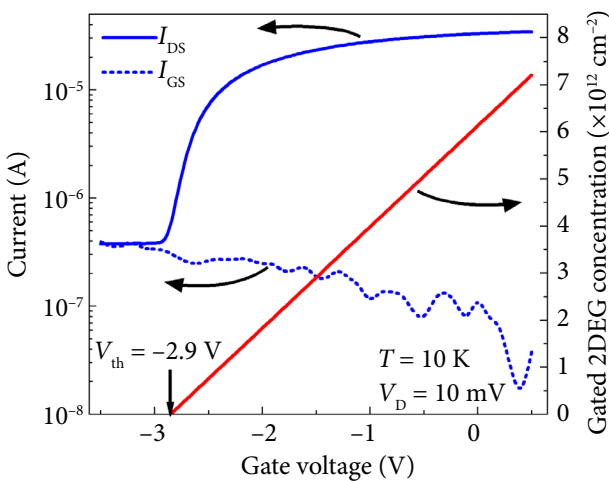


Fig. 3. Transfer current–voltage characteristics ( $I_{\text{DS}}$  is drain current,  $I_{\text{GS}}$  is gate leakage current) and the gate voltage dependence of 2DEG density in the S2 structure at 10 K, drain-to-source voltage  $V_{\text{D}} = 10 \text{ mV}$ , where  $V_{\text{th}} = -2.9 \text{ V}$  is the threshold voltage.

onstrates the transistor-like behaviour with a small gate leakage current density  $J_{\text{GS}} < 2.5 \cdot 10^{-7} \text{ A/mm}^2$ . In analogy to the single-gate FET, the application of voltage  $V_{\text{G}}$  between the grating electrodes (circuited on the common bus) and source terminal ensures an effective control of the 2DEG density in the gated regions of PC structure. The 2DEG density in the gated part of our FET-like structures can be evaluated using the so-called ‘gradual channel’ approximation with known values of the threshold voltage ( $V_{\text{th}}$ ) of the channel depletion

$$n_{\text{G}} = \frac{\epsilon_{\text{bar}} \epsilon_0 V_0}{ed}, \quad (3)$$

where  $V_0 = V_{\text{G}} - V_{\text{th}}$  is the gate voltage swing. From the transfer current–voltage characteristic (solid blue curve in Fig. 2) we found that  $V_{\text{th}} = -2.9 \pm 0.3 \text{ V}$ . Using this value, as well as the values of dielectric permittivity  $\epsilon_{\text{bar}} = 8.9$  and thickness  $d = 22 \text{ nm}$  of the AlGaIn barrier layer, we found the dependence  $n_{\text{G}}(V_{\text{G}})$  which is plotted in Fig. 3 by a red line, where the equilibrium value  $n_{\text{G}}(V_{\text{G}} = 0) = 6.2 \pm 0.6 \times 10^{12} \text{ cm}^{-2}$ . The 2DEG density in the ungated regions  $n_0$  was found from the characterization of bare AlGaIn/GaN heterostructures by capacitance–voltage measurements at 10 kHz using a mercury probe. The extracted value was  $n_0 = 8.7 \pm 0.9 \times 10^{12} \text{ cm}^{-2}$  for the room temperature.

To analyze the plasmon resonances in the biased grating-gate PCs of arbitrary grating filling factor, we use a rigorous approach based on electrodynamic simulations. This method is based on the numerical solutions of Maxwell’s equations, and it operates within the framework of the integral equations method, developed in Refs. [21, 27]. Essentially, the IEM relies on the Green function formalism and involves the reduction of Maxwell’s system of equations to a set of linear integral equations in the coordinate space. These integral equations are amenable to the solution using methods such as Galerkin schemes. It is worth noting that, in contrast to well-established Fourier-modal techniques [30] that are widely utilized, the IEM offers distinct advantages. Notably, it provides a significantly enhanced computational efficiency and ensures the convergence of results with a specified level of accuracy. These qualities render the IEM an excellent choice for our comprehensive analysis of the interaction of plasmonic structures with THz radiation.

Figure 4 demonstrates the calculated contour plot of THz transmittance in the plane ‘gate voltage swing – frequency’ in the wide frequency range 0.1–12 THz for the parameters of the S2 sample. In the region above the threshold voltage,  $V_0 > 0$ , the transmission spectra possess multiple resonances which can be attributed to the resonant excitation of 2D plasmon oscillations of different orders in 2DEG with a spatially modulated profile of electron concentration. We call this regime the delocalized phase of PC when plasmons oscillate in the whole period of the grating-gate coupler consisting of gated and ungated regions.

For the case of weakly modulated 2DEG ( $V_0 = 3$  V,  $n_G = 6.2 \times 10^{12}$  cm $^{-2}$ ), we can identify the most intense fundamental and less intense 2nd and 3rd order plasmon resonances. We observe that the quality factor of the resonances decreases with an increase of their order. With an increase of 2DEG modulation, these resonances are red-shifted and the resonances of a higher order appear. For example, in the intermediate case of 2DEG modulation ( $V_0 = 1$  V,  $n_G = 1.9 \times 10^{12}$  cm $^{-2}$ ), even six resonances are clearly identified. The intensity of these resonances also subsides with an increase of their order. With further approaching of the channel depletion in the gated parts ( $V_0 \rightarrow 0$  V), the transmittance exhibits a multi-res-

onant structure and we can observe the formation of a quasi-continuous plasmonic band.

At near-threshold voltages, close to  $V_0 = 0$ , the contour plot in Fig. 4 demonstrates the gradual transition to another regime. At the strong modulation of 2DEG ( $V_0 = -0.2$  V,  $n_G = 0.43 \times 10^{12}$  cm $^{-2}$ ), the new phase of PC starts to form. At this, the lower-frequency wing of the shown spectral characteristics still experiences the dense frequency modulation. However, at the sub-threshold voltage  $V_0 = -0.1$  V, when the gated region of 2DEG is totally depleted and 2DEG-strip grating has already formed, we observe two orders of the plasmon resonance in the considered frequency range. The most intense fundamental resonance occurs at 2.3 THz and the less intense second-order resonance is realized at 6.12 THz. These plasmon resonances are associated with plasmons in the ungated regions of 2DEG [20, 31, 32]. Even under such conditions, these observations suggest that the phenomena cannot be elucidated solely through the lens of a single-cavity model, see the positions of the horizontal dash-dotted lines calculated by Eq. (2) as for the totally ungated 2D plasmons, taking  $|k| = \pi(2j - 1)/L_0$  ( $j = 1, 2, 3, \dots$ ) as a wave vector defined by the length of the ungated plasmonic cavity. Thus, we call this regime the localized PC phase. Note, in the calculations of part of the contour plot in Fig. 4 relating to

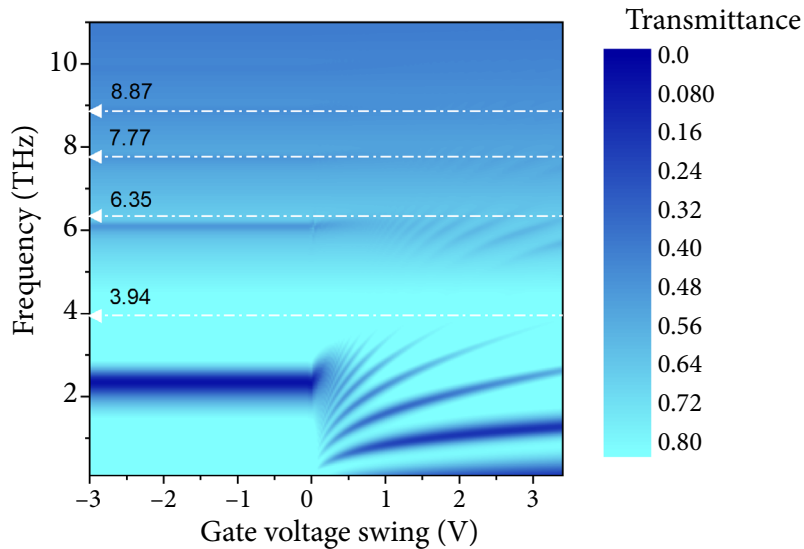


Fig. 4. Calculated contour plot of the transmittance by IEM for the parameters of the S2 sample. The positions of horizontal dash-dotted lines are calculated by Eq. (2) using single-cavity approximations (see below).

the sub-threshold regime, we assumed that  $n_G = 0$  and  $\Delta x = 0$ .

Figure 5 shows the experimental contour plot of the transmission spectrum for the S2 sample. Dashed lines show the positions of the minima obtained as a result of the simulation (fitting) for corresponding samples. To fit experimental data above the threshold voltage,  $V_0 > 0$ , we independently varied two parameters: the concentration of 2DEG under the metallic grating gate  $n_G$  and under the grating opening  $n_O$ . At sub-threshold voltages,  $V_0 < 0$ , we varied  $\Delta x(L_O)$  at a constant value of  $n_O$  and  $n_G$  of  $\sim 0$ .

The plot in Fig. 5 allows us to follow the dependences of plasmonic resonances on frequency and gate voltage. Calculations in Fig. 4 predict the exist-

ence of 5–6 resonances. Two of them can be clearly identified for the S2 sample. At  $V_0 \geq 1$  V, the lowest frequency resonance is most intense and corresponds to the fundamental plasmon resonance marked by (1). The resonances enumerated as (2) and (3) are realized at the higher frequencies and they are less intense. At a decrease of  $V_0$ , the resonances are red-shifted with the emergence of additional resonances. In the narrow region of the near-threshold voltages,  $V_0 \sim -0.3$  to  $-0.6$  V, the gradual transition between the delocalized and localized phases can be identified.

Below the threshold voltages, from  $V_0 = -0.6$  to  $-6$  V, an unexpected linear increase in the frequency of this resonance with saturation at high

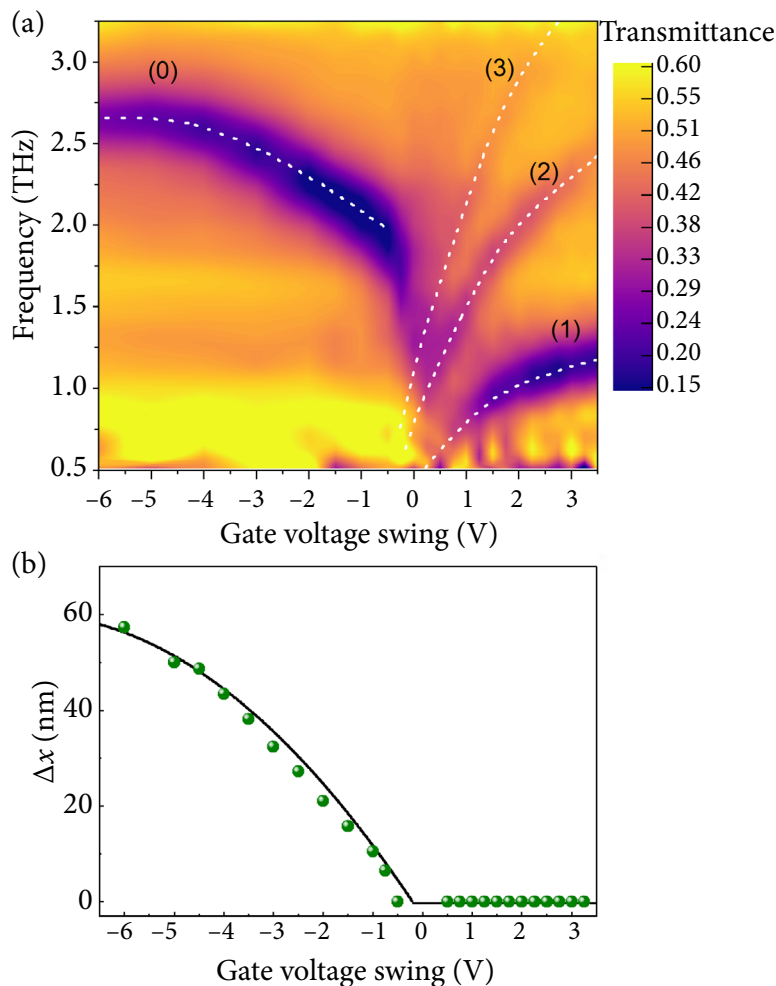


Fig. 5. Measured contour plot of the S2 sample transmittance (a). Dashed curves show the positions of the transmission minima extracted from the calculations by IEM taking into account the additional lateral depletion of ungated regions by  $\Delta x$  value. The obtained  $\Delta x(V_0)$  dependence as a result of the best fitting procedure is shown in panel (b) by dots, and the solid line is a guide for the eye.

gate voltages starting from  $V_0 = -4$  V is observed. It was related to the electrically-induced ‘shrinking’ of the ungated region – the so-called ‘edge gating’ effect [33, 34] (see  $\Delta x$  notation in Fig. 1). Taking into account the dependence of  $\Delta x$  vs  $V_0$  (shown in Fig. 5(b) and obtained as a result of the best fitting procedure), the general features of the calculated mapping are well traced in the contour plot on the basis of experimental data in Fig. 5.

Additionally, we used the finite element method (FEM) to validate independently the obtained IEM results. We employed COMSOL Multiphysics. In particular, the Wave Optics module was used to solve Maxwell’s equations for the assumed above plasmonic structure S2. In order to simulate the delta-thin layers of grating and 2DEG one can use the surface current density boundary condition. However, we decided to go beyond this approximation and considered those layers as 3D

parts of the structure. That gave us the possibility not only to validate our implementation of IEM but also to check the applicability of delta-thin layer approximation. Therefore, we fixed the thickness of the 2DEG layer to  $\eta_{2\text{DEG}} = 3$  nm and the thickness of the grating metal to  $\eta_{\text{GR}} = 50$  nm. Considering the value of  $\eta$ , the 3D conductivity was converted into 2D as following  $\sigma_{3\text{D}} = \sigma_{2\text{D}}/\eta$ .

As seen from Fig. 6, FEM and IEM provide the same results in transmittance as well as in reflectance and absorptance spectra for different values of 2DEG modulation at  $V_0 = 3, 0.1$  and  $-0.1$  V. The relative errors between these methods do not exceed 1% for all comparative curves in panels (a) and (b), and 2.5% for panel (c) in the whole considered frequency range. This validates the developed IEM as well as the applicability of the delta-thin metallic grating and delta-thin electron conductive layer model.

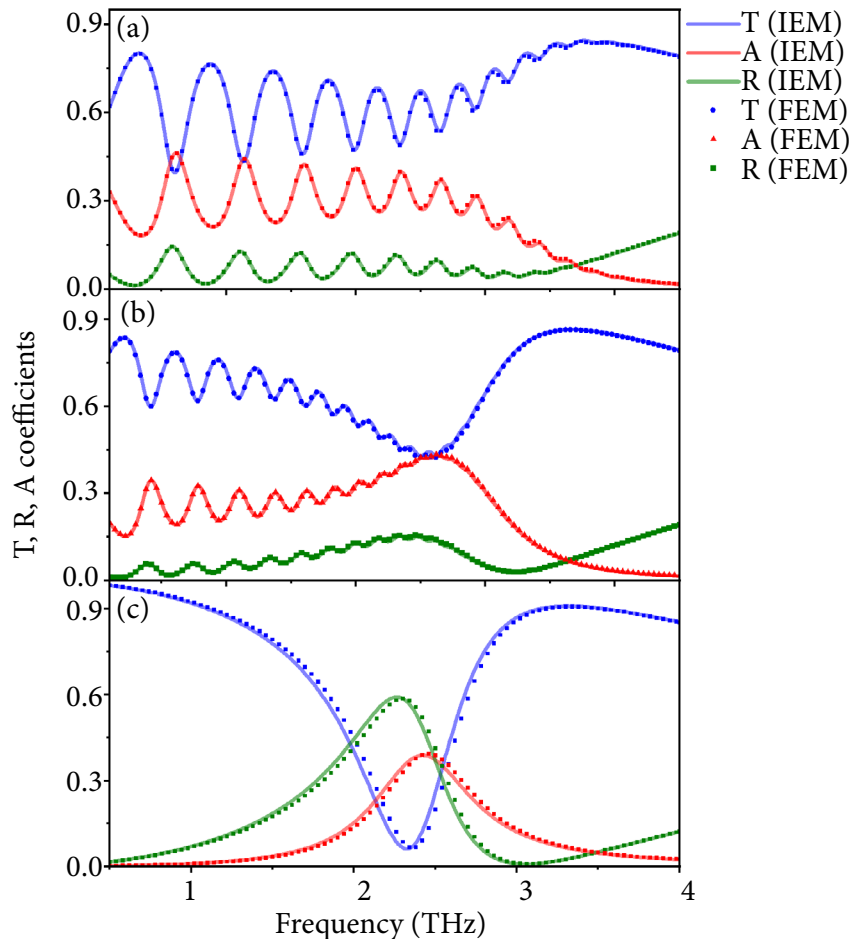


Fig. 6. Transmittance (T), reflectance (R) and absorptance (A) spectra calculated by IEM (solid lines) and FEM (dotted lines). Panels: (a)  $V_0 = 3$  V; (b)  $V_0 = 0.1$  V; (c)  $V_0 = -0.1$  V.

It should be noted that the developed IEM is more effective and more suitable for fast processing of the experimental data than the FEM concerning the computation time. The simultaneous calculation of three curves for T, R, A-coefficients with 500 points per curve requires 1.4 min within IEM. The computation of the same curves using FEM, taking a 10 nm grid, requires 2 h and 30 min at a similar computational power because COMSOL calculates additionally all components of the em fields in the entire simulated structure and at each frequency. While IEM is much faster than FEM, FEM is much more flexible that gives the possibility to add different layers, different shapes of gratings, etc.

#### 4. Near-field study of PC structure

The main difference between delocalized and localized phases can be illustrated in the examples

of the near-field patterns calculated by FEM taking a 10 nm grid for a good spatial resolution (Fig. 7). Particularly, we pay attention to the spatial distributions of the amplitude of  $x$  component of the electric field,  $|E_x(x, z)|$ , the em wave in the vicinity of the metallic grating and 2DEG.

In the case of the delocalized phase, as depicted in panels (a) and (b) of Fig. 7, the em field within the near-field zone surrounding the plasmonic structure exhibits a strong non-uniform distribution. This non-uniformity becomes particularly pronounced in the vicinity of the metallic finger ridges. Additionally, a notable amplification effect is observed in the gated region of 2DEG, where the amplitude  $|E_x|$  experiences a fourfold increase in magnitude compared to the incident wave amplitude ( $E_0$ ). This enhancement can be attributed to the resonant excitation of both the fundamental mode (panel (a)) and the second-order mode (panel (b)) of 2D plasmons.

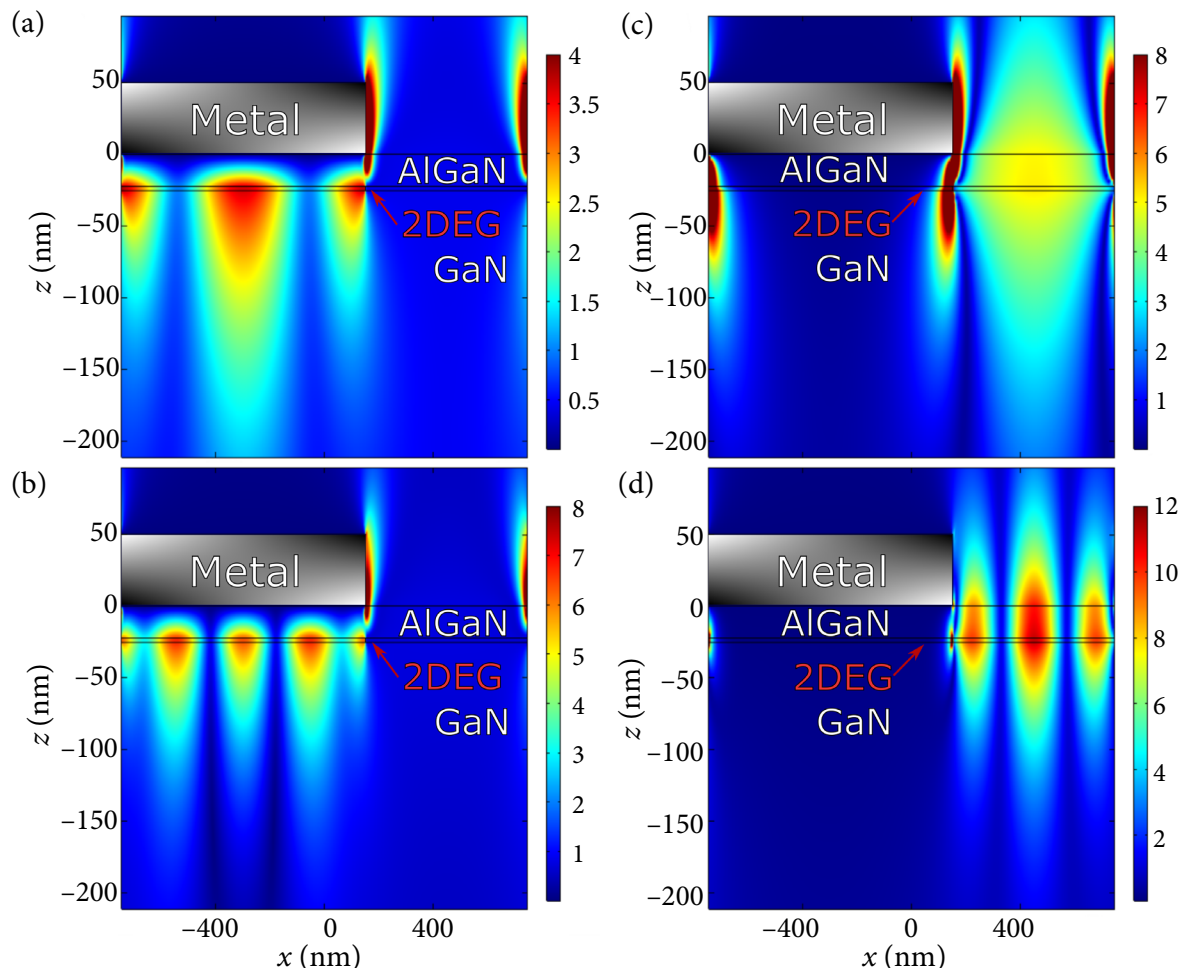


Fig. 7. Spatial distribution of the  $|E_x|/E_0$  component of the em field that corresponds to the first two plasmon resonances at 0.58 THz (a) and 1.11 THz (b) of the delocalized phase, and the first two plasmon resonances at 2.46 THz (c) and 6.15 THz (d) of the localized phase.

The spatial distribution of  $|E_x|$  reveals an oscillatory behaviour within the gated region while exhibiting a nearly constant distribution in the ungated area of 2DEG. Remarkably, these distributions strongly suggest that the gated region of 2DEG functions as a cavity for plasmonic oscillations. Within this cavity, plasmonic oscillations occur in a manner such that the width of the cavity corresponds to odd multiples of half-wavelengths, a phenomenon often associated with a resonant cavity behaviour.

In the localized phase, a distinct pattern emerges in the near-field characteristics, as illustrated in Fig. 7(c, d). In this phase, the concentration of em energy is even more pronounced. Notably, the majority of the em wave energy becomes concentrated within the vicinity of the metallic grating openings. Specifically, regions with elevated energy levels form in close proximity to the ridges of metallic fingers and along the strips of the 2DEG-grating interface. It is important to observe that the em wave does not significantly penetrate beneath the metallic gate, resulting in the formation of a ‘cold zone’ in this region.

The spatial distribution of the  $x$  component of em wave within the 2DEG plane reveals that, in this regime, the ungated section of 2DEG effectively operates as a cavity. Notably, for the fundamental resonance at 2.3 THz, the plasmon oscillations exhibit a half-wavelength localization along the width of the grating opening. For the second-order resonance at 6.12 THz, a clear localization pattern is observed with three half-wavelength localizations. Furthermore, it is evident that the em energy becomes even more strongly localized within the ungated region of 2DEG for the second-order resonance, emphasizing the distinct behaviour of this phase.

## 5. Conclusions

We studied the THz properties of the grating-gate plasmonic crystal structure and demonstrated the electrically controlled gradual transition between two distinct resonant phases observed in transmission spectra. The first, delocalized phase, occurs at weakly modulated 2DEG. This phase is associated with the emergence of several resonances in transmission spectra corresponding to different orders of 2D plasmon excitations in weak-

ly non-uniform 2D plasma. With an increase of the modulation degree, the phase transition occurs and a localized phase starts to form. It is connected with plasmon excitations exclusively in the ungated parts of 2DEG.

THz transmission spectra of all types of plasmon resonance in the grating-gate structures were calculated by the integral equation method used for the numerical solution of Maxwell’s equations. Additionally, the results were validated independently by the finite element method, which was also used for the calculations of spatial distributions of the electric field components of electromagnetic waves in the near-field zone.

The near-field calculations provide valuable insights into the fundamental physical distinctions between the two discovered phases of plasmonic crystals. In the delocalized phase, the plasmonic absorption of electromagnetic energy takes place in both gated and ungated parts of 2DEG, but with a domination of the gated part. In the localized phase, the plasmon excitation is primarily localized in the ungated region of 2DEG. The plasmonic absorption of the THz wave takes place exclusively in the ungated part of 2DEG, indicating a main physical diversity from the delocalized phase.

We suggest that the performed experimental and theoretical analysis of the plasmonic crystal phases and the transition between them, including interpretation of their physical nature on the language of near-field patterns, provides a deep insight into the research of resonant properties of the electrically controlled plasmonic crystal structure. It is important to stress that our results have general significance and can extend their relevance to other semiconductor-based structures, offering broader applications in the field of THz plasmonics.

## Acknowledgements

This work was supported by the ‘International Research Agendas’ Program of the Foundation for Polish Science, co-financed by the European Union under the European Regional Development Fund for CENTERA Lab (No. MAB/2018/9) and co-funded by the European Union (ERC ‘TERA-PLASM’, Project No. 101053716). Views and opinions expressed are, however, those of the author(s) only and do not necessarily reflect those of the European Union or the European Research Council.

Neither the European Union nor the granting authority can be held responsible for them. P. S. is grateful for the partial support provided by the National Science Centre, Poland allocated on the basis of Grant No. 2019/35/N/ST7/00203. V.V.K. and S.M.K. acknowledge the long-term program of support of the Ukrainian research teams at the Polish Academy of Sciences carried out in collaboration with the U.S. National Academy of Sciences with the financial support of external partners. S.M.K. is grateful to Technical University of Dortmund, where COMSOL calculations were performed.

## References

- [1] M. Dyakonov and M. Shur, Shallow water analogy for a ballistic field effect transistor: New mechanism of plasma wave generation by dc current, *Phys. Rev. Lett.* **71**, 2465 (1993).
- [2] W. Knap, Y. Deng, S. Rumyantsev, and M. Shur, Resonant detection of subterahertz and terahertz radiation by plasma waves in submicron field-effect transistors, *Appl. Phys. Lett.* **81**, 4637–4639 (2002).
- [3] J.A. Delgado-Notario, W. Knap, V. Clericò, J. Salvador-Sánchez, J. Calvo-Gallego, T. Taniguchi, K. Watanabe, T. Otsuji, V.V. Popov, and D.V. Fateev, Enhanced terahertz detection of multigate graphene nanostructures, *Nanophotonics* **11**, 519–529 (2022).
- [4] E. Shaner, M. Lee, M. Wanke, A. Grine, J. Reno, and S.J. Allen, Single-quantum-well grating-gated terahertz plasmon detectors, *Appl. Phys. Lett.* **87**, 193507 (2005).
- [5] D. Coquillat, S. Nadar, F. Teppe, N. Dyakonova, S. Boubanga-Tombet, W. Knap, T. Nishimura, T. Otsuji, Y. Meziani, and G. Tsymbalov, Room temperature detection of sub-terahertz radiation in double-grating-gate transistors, *Opt. Express* **18**, 6024–6032 (2010).
- [6] P. Sai, S.O. Potashin, M. Szoła, D. Yavorskiy, G. Cywiński, P. Prystawko, J. Łusakowski, S.D. Ganichev, S. Rumyantsev, W. Knap, and V.Y. Kachorovskii, Beatings of ratchet current magneto-oscillations in GaN-based grating gate structures: Manifestation of spin-orbit band splitting, *Phys. Rev. B* **104**, 045301 (2021).
- [7] T. Onishi, T. Tanigawa, and S. Takigawa, High power terahertz emission from a single gate AlGaIn/GaN field effect transistor with periodic Ohmic contacts for plasmon coupling, *Appl. Phys. Lett.* **97**, 092117 (2010).
- [8] V.A. Shalygin, M.D. Moldavskaya, M.Y. Vinnichenko, K.V. Maremyanin, A.A. Artemyev, V.Y. Panevin, L.E. Vorobjev, D.A. Firsov, V.V. Korotyeyev, A.V. Sakharov, E.E. Zavarin, D.S. Arteev, W.V. Lundin, A.F. Tsatsulnikov, S. Suihkonen, and C. Kauppinen, Selective terahertz emission due to electrically excited 2D plasmons in AlGaIn/GaN heterostructure, *J. Appl. Phys.* **126**, 183104 (2019).
- [9] S. Boubanga-Tombet, W. Knap, D. Yadav, A. Sattou, D.B. But, V.V. Popov, I.V. Gorbenko, V. Kachorovskii, and T. Otsuji, Room-temperature amplification of terahertz radiation by grating-gate graphene structures, *Phys. Rev. X* **10**, 031004 (2020).
- [10] V.Y. Kachorovskii and M. Shur, Current-induced terahertz oscillations in plasmonic crystal, *Appl. Phys. Lett.* **100**, 232108 (2012).
- [11] A.S. Petrov, D. Svintsov, V. Ryzhii, and M.S. Shur, Amplified-reflection plasmon instabilities in grating-gate plasmonic crystals, *Phys. Rev. B* **95**, 045405 (2017).
- [12] S. Allen Jr, D. Tsui, and R. Logan, Observation of the two-dimensional plasmon in silicon inversion layers, *Phys. Rev. Lett.* **38**, 980 (1977).
- [13] D. Tsui, S. Allen Jr, R. Logan, A. Kamgar, and S. Coppersmith, High frequency conductivity in silicon inversion layers: Drude relaxation, 2D plasmons and minigaps in a surface superlattice, *Surf. Sci.* **73**, 419–433 (1978).
- [14] N. Nader Esfahani, R. Peale, W. Buchwald, C. Fredrickson, J. Hendrickson, and J. Cleary, Millimeter-wave photoresponse due to excitation of two-dimensional plasmons in InGaAs/InP high-electron-mobility transistors, *J. Appl. Phys.* **114**, 033105 (2013).
- [15] M. Białek, M. Czapkiewicz, J. Wróbel, V. Umansky, and J. Łusakowski, Plasmon dispersions in high electron mobility terahertz detectors, *Appl. Phys. Lett.* **104**, 263514 (2014).
- [16] A. Muravjov, D. Veksler, V. Popov, O. Polischuk, N. Pala, X. Hu, R. Gaska, H. Saxena, R. Peale, and

- M. Shur, Temperature dependence of plasmonic terahertz absorption in grating-gate gallium-nitride transistor structures, *Appl. Phys. Lett.* **96**, 042105 (2010).
- [17] M. Dub, D. But, P. Sai, Y. Ivonyak, M. Słowikowski, M. Filipiak, G. Cywinski, W. Knap, and S. Rumyantsev, Plasmons in AlGaN/GaN grating-gate structure probing with 300 K background illumination, *AIP Adv.* **13**, 095017 (2023).
- [18] H. Yan, X. Li, B. Chandra, G. Tulevski, Y. Wu, M. Freitag, W. Zhu, P. Avouris, and F. Xia, Tunable infrared plasmonic devices using graphene/insulator stacks, *Nat. Nanotechnol.* **7**, 330–334 (2012).
- [19] Y. Li, P. Ferreyra, A.K. Swan, and R. Paiella, Current-driven terahertz light emission from graphene plasmonic oscillations, *ACS Photonics* **6**, 2562–2569 (2019).
- [20] S.A. Mikhailov, Plasma instability and amplification of electromagnetic waves in low-dimensional electron systems, *Phys. Rev. B* **58**, 1517 (1998).
- [21] D.V. Fateev, V.V. Popov, and M.S. Shur, Transformation of the plasmon spectrum in a grating-gate transistor structure with spatially modulated two-dimensional electron channel, *Semiconductors* **44**, 1406–1413 (2010).
- [22] V.V. Popov, Plasmon excitation and plasmonic detection of terahertz radiation in the grating-gate field-effect-transistor structures, *J. Infrared Millim. Terahertz Waves* **32**, 1178–1191 (2011).
- [23] Y.M. Lyaschuk and V. Korotyeyev, Theory of detection of terahertz radiation in hybrid plasmonic structures with drifting electron gas, *Ukr. J. Phys.* **62**, 889–889 (2017).
- [24] Y.M. Lyaschuk, S.M. Kukhtaruk, V. Janonis, and V.V. Korotyeyev, Modified rigorous coupled-wave analysis for grating-based plasmonic structures with a delta-thin conductive channel: far-and near-field study, *JOSA A* **38**, 157–167 (2021).
- [25] V. Korotyeyev and V. Kochelap, Plasma wave oscillations in a nonequilibrium two-dimensional electron gas: electric field induced plasmon instability in the terahertz frequency range, *Phys. Rev. B* **101**, 235420 (2020).
- [26] V.V. Korotyeyev, V.A. Kochelap, V.V. Kaliuzhnyi, and A.E. Belyaev, High-frequency conductivity and temperature dependence of electron effective mass in AlGaN/GaN heterostructures, *Appl. Phys. Lett.* **120**, 252103 (2022).
- [27] P. Sai, V.V. Korotyeyev, M. Dub, M. Słowikowski, M. Filipiak, D.B. But, Y. Ivonyak, M. Sakowicz, Y.M. Lyaschuk, S.M. Kukhtaruk, G. Cywiński, and W. Knap, Electrical tuning of terahertz plasmonic crystal phases, *Phys. Rev. X* **13**, 041003 (2023).
- [28] A. Chaplik, Possible crystallization of charge carriers in low-density inversion layers, *Sov. Phys. JETP* **35**, 395 (1972).
- [29] N. Okisu, Y. Sambe, and T. Kobayashi, Far-infrared emission from two-dimensional plasmons in AlGaAs/GaAs heterointerfaces, *Appl. Phys. Lett.* **48**, 776–778 (1986).
- [30] V. Ryzhii, T. Otsuji, and M. Shur, Graphene based plasma-wave devices for terahertz applications, *Appl. Phys. Lett.* **116**, 140501 (2020).
- [31] W. Schaich, Analysis of a special model for a grating coupler, *Phys. Rev. B* **62**, 2721 (2000).
- [32] T.L. Zinenko, A. Matsushima, and A.I. Nosich, Surface-plasmon, grating-mode, and slab-mode resonances in the H- and E-polarized THz wave scattering by a graphene strip grating embedded into a dielectric slab, *IEEE J. Sel. Top. Quantum Electron.* **23**, 1–9 (2017).
- [33] G. Cywiński, I. Yahniuk, P. Kruszewski, M. Grabowski, K. Nowakowski-Szkudlarek, P. Prystawko, P. Sai, W. Knap, G. Simin, and S. Rumyantsev, Electrically controlled wire-channel GaN/AlGaIn transistor for terahertz plasma applications, *Appl. Phys. Lett.* **112**, 133502 (2018).
- [34] P. Sai, D. But, I. Yahniuk, M. Grabowski, M. Sakowicz, P. Kruszewski, P. Prystawko, A. Khachapuridze, K. Nowakowski-Szkudlarek, and J. Przybytek, AlGaIn/GaN field effect transistor with two lateral Schottky barrier gates towards resonant detection in sub-mm range, *Semicond. Sci. Technol.* **34**, 024002 (2019).

**GARDELĖS-UŽTŪROS PLAZMONINIŲ KRISTALŲ TERAHERCINĖS SAVYBĖS**

P. Sai <sup>a\*</sup>, M. Dub <sup>a</sup>, V. Korotyeyev <sup>a,b</sup>, S. Kukhtaruk <sup>a,b</sup>, G. Cywinski <sup>a</sup>, W. Knap <sup>a</sup>

<sup>a</sup> *Lenkijos MA Aukštojo slėgio fizikos instituto CENTERA laboratorijos, Varšuva, Lenkija*

<sup>b</sup> *Ukrainos nacionalinės MA V. Laškariovo puslaidininkų fizikos institutas, Kyjivas, Ukraina*

**Special dedication to prof. Gintaras Valušis**

Gintaras is an example of the exceptional human being who can join together high level scientific activity with efficient and researchers-friendly science management. He is also a friend and collaborator that you always can count on. I count on continuous collaboration with him and his team and maybe one day we will reach our many years dream of constructing Lithuanian–Polish Common Research Center on THz science and technology.

Prof. Dr. Hab. Wojciech Knap  
Institute of High Pressure Physics (IHPP)  
Warsaw, Poland